Radioimmunoimaging of ^{125}I-labeled anti-CD93 monoclonal antibodies in a xenograft model of non-small cell lung cancer

WEIWEI LIU, CHAO ZHANG, HUI CAO, DAI SHI, SHANSHAN ZHAO, TING LIANG and GUIHUA HOU

Biomedical Isotope Research Center, School of Basic Medical Sciences, Shandong University, Jinan, Shandong 250012, P.R. China

Received October 26, 2018; Accepted September 9, 2019

DOI: 10.3892/ol.2019.11036

Abstract. Lung cancer, especially non-small cell lung cancer (NSCLC), is the most common malignant tumor associated with poor prognosis. Angiogenesis plays a vital role in NSCLC, and could be used in tumor staging and therapy evaluation. CD93 (C1q receptor) is reportedly a key regulator of tumor angiogenesis. In the present study, the efficacy and specificity of a ^{125}I-labeled CD93-specific monoclonal antibody (^{125}I-anti-CD93 mAb) in detecting NSCLC xenografts were analyzed, and the association between CD93 expression and ^{125}I-anti-CD93 mAb uptake by tumors was evaluated. The targeting ability of ^{125}I-anti-CD93 mAb enabled its rapid, continuous and highly specific accumulation in CD93-expressing tumors *in vivo*. These results revealed the potential applicability of ^{125}I-anti-CD93 mAb for non-invasive imaging diagnosis of CD93-positive NSCLC.

Introduction

Lung cancer is the most common type of malignant tumor, with a high incidence of ~2.1 million new cases and ~1.8 million deaths of lung cancer in 2018 worldwide (1-3). Non-small cell lung cancer (NSCLC) accounts for 15% of all cases of lung cancer with multiple toxin-associated mutations, including epidermal growth factor, KRAS, PI3K subunit α (PIK3CA) and AKT1 mutations and PIK3CA amplification (4-6). Cancer therapy has become increasingly personalized over the past decade (7-9), and new effective diagnostic methods and evaluation systems are urgently needed for imaging malignancies and monitoring their therapeutic responses.

Correspondence to: Professor Ting Liang or Professor Guihua Hou, Biomedical Isotope Research Center, School of Basic Medical Sciences, Shandong University, 44 Wenhua Xi Road, Jinan, Shandong 250012, P.R. China
E-mail: liangting@sdu.edu.cn
E-mail: ghhou@sdu.edu.cn

Key words: CD93, non-small cell lung cancer, radioimmunoimaging, ^{125}I-anti-CD93 monoclonal antibody, phosphor autoradiography

Imaging technologies allow non-invasive diagnosis of cancers and provide dynamic information on the effectiveness of therapies and on patient prognosis. Cancer diagnosis by conventional radiological imaging methods, such as computed tomography (CT) or magnetic resonance imaging (MRI) scanning, is not fully straightforward in certain cases due to the relatively non-specific nature of the clinical features and incomplete validation of imaging findings (10). Molecular imaging has shown great potential in the cancer field and has provided detailed information about the uptake of target molecules by numerous types of tumor lesions and their presence therein. The most common application to date has been the imaging of overexpressed antigen-associated tumors; the radiolabeled antibody of the human epidermal growth factor receptors (HER1, HER2 and HER3) have been widely used in breast cancer, gastric cancer and NSCLC (11,12). Compared with traditional imaging techniques such as CT or MRI, molecular imaging in nuclear medicine is a non-invasive whole-body scanning modality, and is more suitable for the detection and quantification of the expression levels of target molecules in tumor tissue (13,14). Radioimmunoimaging, which involves the use of a radionuclide in combination with highly specific antibody-based imaging tracers (15), can provide a non-invasive way to evaluate the expression and distribution of molecular targets *in vivo*, thereby contributing to accurate disease diagnosis and therapeutic and prognostic evaluations. Therefore, the search for molecular markers that are highly specific to the various cancer types is of great importance and urgently required for radioimmunoimaging.

Angiogenesis is of fundamental importance for growing tumors (16,17) since by switching to an angiogenic phenotype, followed by the development of new vasculature, solid tumors can reach a critical size of 1-2 mm^3 (18,19). Thus, angiogenesis is an attractive and novel target for tumor diagnosis.

CD93, a transmembrane protein, acts as an adhesion molecule to promote the adhesion and migration of inflammatory cells to endothelial cells, the phagocytosis of apoptotic cells, and the formation of new blood vessels (20). Previous studies have shown CD93 to be a key regulator of tumor angiogenesis, regulating adhesion between the cells and the cellular matrix. Decreased expression of CD93 could induce cytoskeletal reconstruction and adhesion loss, thereby inhibiting endothelial cell adhesion and migration, as well as abnormal angiogenesis in glioblastoma (21,22). Additionally, CD93 has

low expression in normal tissue, but differential expression in metastatic and advanced primary glioma, indicating its potential use in cancer diagnosis (23).

In the present study, a ^{125}I-labeled CD93-specific monoclonal antibody (^{125}I-anti-CD93 mAb) was prepared for the investigation of CD93 expression in mouse xenograft models of two different types of NSCLC cell lines. We postulated that ^{125}I-anti-CD93 mAb radioimmunoimaging could be used for monitoring NSCLC cells with CD93-positive expression, and therefore may be useful in the future for non-invasive clinical diagnosis of this disease.

Materials and methods

Ethics statement. All animal studies were conducted in accordance with protocols approved by the Animal Care and Use Committee of Shandong University.

Cell culture. The human lung adenocarcinoma (LUAD) A549 cell line and the human lung squamous cell carcinoma (LUSC) SK-MES-1 cell line (both human NSCLC cell lines) were obtained from the American Type Culture Collection. Both cell lines were cultured in RPMI-1640 medium supplemented with 10% fetal bovine serum (Gibco; Thermo Fisher Scientific, Inc.) and 1% penicillin/streptomycin (HyClone; GE Healthcare Life Sciences) at 37˚C in a humidified incubator with 5% CO_2.

Flow cytometry analysis of CD93 expression in NSCLC cells. CD93 expression in A549 and SK-MES-1 cells was determined using flow cytometry. In brief, the cells were digested by trypsin, centrifuged (100 x g at 4˚C for 5 min) and suspended in ice-cold PBS (pH 7.4) at a concentration of $5x10^5$ cells/100 μl. The cells were then incubated with PBS and phycoerythrin (PE)-conjugated CD93 antibody (200 μg/ml, dissolved in phosphate-buffered solution with 0.09% sodium azide and 0.2% BSA, pH 7.2; BioLegend, Inc.) for 30 min at 4˚C. After the incubation, the cells were washed twice with ice-cold PBS and the binding efficiency was analyzed using a MACSQuant flow cytometer (Miltenyi Biotec GmbH). The mean fluorescence intensities were quantified using FlowJo 7.6.1 software (Tree Star, Inc.).

Quantification of CD93 mRNA and protein expression levels. The CD93 mRNA and protein expression levels were evaluated using semi-quantitative reverse transcription (RT)-PCR and western blot assays, respectively.

For the semi-quantitative RT-PCR analysis, cells at ~70% confluency were digested by trypsin and centrifuged (100 x g at 4˚C for 5 min), and the total RNA was extracted using TRIzol® (Invitrogen; Thermo Fisher Scientific, Inc.) according to the manufacturer's instructions. Total RNA was resuspended in RNase-free water. Subsequently, the first-strand DNA was generated using TransScript® One-Step gDNA Removal and cDNA Synthesis kits (Beijing Transgen Biotech, Co., Ltd.). The reactions were performed in a total volume of 20 μl, consisting of 1 μg total RNA, 1 μl anchored oligo(dT)18 (0.5 μg/μl), 10 μl 2X TransScript reaction mix, 1 μl reverse transcription enzyme mix and 7 μl RNase-free water, and incubated at 42˚C for 30 min and 85˚C for 5 min. According to the operation instruction of EasyTaq PCR kit (Beijing Transgen Biotech, Co., Ltd.), 2 μl complementary DNA was mixed with 0.5 μl specific primers (10 μM), 2 μl dNTP (2.5 mM), 0.25 μl EasyTaq DNA polymerase, 2.5 μl 10X EasyTaq buffer and 17.25 μl double-distilled water. The PCR primer sequences used are as follows: CD93 forward, 5'-TGCCTGGACCCT AGTCTGC-3' and reverse, 5'-GCTTGGAGATGCACGAGT TC-3'; and GAPDH forward, 5'-GGAGCGAGATCCCTC CAAAAT-3' and reverse, 5'-GGCTGTTGTCATACTTCT CATGG-3'. GAPDH was used as the control. The PCR conditions were as follows: Initial denaturation at 94˚C for 3 min, followed by 35 cycles of 94˚C for 30 sec, 56˚C for 30 sec and 72˚C for 1 min, with a final extension at 72˚C for 10 min. The PCR products were electrophoresed in 1.5% (w/v) agarose gels containing 0.5 μg/ml ethidium bromide to confirm the expected size of the fragments and were visualized under UV light. Band density was analyzed and quantified using Gel-Pro 3.1 software (Media Cybernetics, Inc.).

For the western blot analysis, A549 and SK-MES-1 cells at ~70% confluency were harvested by scraping and the total protein was extracted using RIPA lysis buffer containing 1% phenylmethylsulfonyl fluoride (Boston BioProducts, Inc.). The protein concentration was determined with a protein assay kit (Beyotime Institute of Biotechnology). Then, 20 μg total protein was loaded onto the corresponding wells of 4-12% SDS-PAGE (Bio-Rad Laboratories, Inc.) together with the Chameleon Duo Pre-stained Protein Ladder (SMOBIO Technology, Inc.). The electrophoresed proteins were transferred onto a 0.45-μm PVDF membrane (EMD Millipore) at 100 mV for 90 min at 4˚C in transfer buffer (25 mM Tris, 0.2 M glycine and 20% methanol). The membrane was blocked in 5% (w/v) skimmed milk blocking buffer for 1 h at 20˚C with agitation and then washed with TBS containing Tween-20 (TBS-T). Rabbit anti-human CD93 antibody (dilution, 1:1,000; dissolved in 40% glycerol, 9.85% Tris glycine and 50% tissue culture supernatant, pH 7.4; cat. no. ab134079; Abcam) was added and the membrane was incubated overnight at 4˚C. GAPDH polyclonal antibody (dilution, 1:5,000; dissolved in phosphate-buffered solution with 0.02% sodium azide and 50% glycerol, pH 7.2; cat. no. AB0063; Bioworld Technology, Inc.) was used as the loading control. Next, the membrane was washed 3 times with TBS-T and then incubated with horseradish peroxidase (HRP)-conjugated goat anti-rabbit IgG (dilution 1:10,000; dissolved in phosphate-buffered solution with 0.09% sodium azide and 0.2% BSA, pH 7.2; cat. no. TA140003; OriGene Technologies, Inc.) for 1 h at 20˚C. After washing with TBS-T, Immobilon Western HRP Substrate (EMD Millipore) was added. The membrane was subsequently scanned and quantitatively analyzed using a Tanon 4200 imaging system (Tanon Science & Technology Co., Ltd.) and ImageJ 1.8.0 software (National Institutes of Health).

Preparation of the ^{125}I-anti-CD93 mAb. Radioiodination of anti-CD93 mAb and rabbit isotype IgG (dissolved in 0.01% sodium azide, 59% PBS, 40% glycerol and 0.05% BSA, pH 7.2; cat. nos. ab134079 and ab172730; Abcam) with $Na^{125}I$ was performed according to the Iodogen solid-phase labeling method, as previously described (24). In brief, 10 μg anti-CD93 mAb was added to 100 μl phosphate buffer (PB; 0.05 M; pH 7.4), and then 12 megabecquerel (MBq; 12

MBq=300 mCi) $Na^{125}I$ was added. The mixture was incubated for 20 min at 37˚C, and the reaction was subsequently terminated by adding 150 μl 0.05 M PB and incubating the mixture for 10 min at 37˚C. The labeling compound was purified on a Sephadex G-25 gel filtration column (GE Healthcare Life Sciences) as previously described (25) and the labeling efficiency was calculated. A mixture of 0.9% saline and methanol at a volume ratio of 1:2 was used as an unfolding agent. The stability of ^{125}I-anti-CD93 mAb *in vitro* was determined in 0.05 M PBS (pH 7.4) or in human serum. The ^{125}I-labeled IgG isotype was used as a non-specific control tracer and was prepared in a similar method as aforementioned.

Evaluation of ^{125}I-anti-CD93 mAb. The binding affinity of ^{125}I-anti-CD93 mAb to A549 and SK-MES-1 cells was determined. In brief, cells were seeded into 96-well culture plates at $1x10^5$ cells/well. ^{125}I-anti-CD93 mAb in PBS solution (at concentrations ranging from 3 to 100 nM) was added to the cells. After incubation at room temperature for 2 h, the cells were washed twice with ice-cold 1X PBS containing 0.1% BSA (Shanghai Lianshuo Biological Technology Co., Ltd.), pyrolyzed with 1 mol/l NaOH and harvested, and the activity was determined with a CRC 25R gamma counter (Capintec, Inc.). For the competitive binding assay, 0.1-1,000 nM anti-CD93 mAb and 15 nM ^{125}I-anti-CD93 mAb were used, with a final reaction volume of 500 μl. The maximum binding ability (Bmax), dissociation constant (Kd) and receptor density on the cells were determined using GraphPad Prism 5.0 software (GraphPad Software, Inc.).

Animal studies. Subcutaneous xenograft tumors of the A549 or SK-MES-1 cell lines were induced in 240 5-week-old (weight, 18±2 g) female nude mice (BALB/c-nu; n=5/group; Beijing Vital River Laboratory Animal Technology Co., Ltd.) by injecting $2x10^6$ tumor cells (suspended in 200 μl PBS) into the lower right flank of the animal. All mice were bred and maintained under specific pathogen-free conditions in individually ventilated (HEPA-filtered air) sterile cages (14 days; humidity, 50-60%). All mice were maintained under a 12-h light/dark cycle with access to standard mice chow and sterilized water *ad libitum*. The mice and tumor size were monitored every 2 days for 2 weeks (Fig. S1). The volume of the tumor was calculated as (long diameter x short diameter x short diameter)/2. The animals were subjected to imaging and biodistribution studies once the tumor size had reached 5-10 mm in diameter.

Dynamic whole-body phosphor autoradiography. To block hormone synthesis by the thyroid gland, 10% potassium iodide was added to the drinking water 2 days before injection of the radiotracers. Tumor-bearing mice were then intravenously injected with 0.55 MBq ^{125}I-anti-CD93 mAb. ^{125}I-IgG (0.55 MBq) was also injected into another group of A549 tumor-bearing mice as the IgG isotype control for imaging. Phosphor autoradiography scans were conducted at 24, 48 and 72 h post injection. Dynamic whole-body phosphor autoradiography was performed with a Cyclone Plus scanner (PerkinElmer, Inc.). Anesthesia was induced and maintained with pentobarbital sodium (60 mg/kg) by intraperitoneal injection. Each anesthetized mouse was placed on the storage phosphor screen plate, with its back to the plate in low light, and exposed to the plate for 20 min. Upon exposure, the plate was immediately scanned. Semi-quantitative analysis was performed by manually drawing rectangular regions of interest (n=5) within the target area at each time point. Digital light units per square millimeter (DLU/mm^2) measurements were obtained using OptiQuant Image Analysis Software v5.0 (PerkinElmer, Inc.).

Biodistribution studies. ^{125}I-anti-CD93 mAb (0.37 MBq) was injected into each mouse tumor model (n=5 per group). ^{125}I-IgG (0.37 MBq) was also injected in another group of A549 tumor-bearing mice to demonstrate the non-specific distribution of the IgG isotype. The mice were sacrificed by cervical dislocation at 24, 48 and 72 h post injection, and the stopping of the heart and the limbs turning white indicated death. The tumor, blood and major tissues/organs (heart, lung, liver, kidney, spleen, small intestine and muscle) were harvested, washed and weighed. The samples and primed standards used as the radioactive background control were evaluated for radioactivity with the gamma counter, and the measurements were corrected for physical decay using a standard value. Tissue activity was expressed as the percentage of injected dose per gram (% ID/g). The target-to-non-target (T/NT) ratio was defined as the ratio of the tumor to the muscle on the opposite side from the cell injection site.

Statistical analysis. All experiments were repeated three times. All data are denoted as the mean ± SD. The Student's t-test was used to compare the expression of CD93 in A549 and SK-MES-1 cell lines. Statistical comparisons of biodistribution data sets were analyzed using a one-way factorial ANOVA. All analyses were performed with GraphPad Prism v5.0 software (GraphPad Software, Inc.). $P<0.05$ was considered to indicate a statistically significant difference.

Results

Flow cytometry analysis of CD93 expression in the NSCLC cell lines. The two NSCLC cell lines incubated with either PE-conjugated CD93 antibody or negative control PBS were analyzed for CD93 expression using flow cytometry (Fig. 1). The A549 cells displayed enhanced fluorescence signals when incubated with the PE-conjugated CD93 antibody, which was indicative of elevated CD93 expression in this cell line. By contrast, a lower fluorescence signal was detected in the SK-MES-1 cell line.

Quantification of CD93 mRNA and protein expression in the NSCLC cell lines. The relative expression levels of CD93 in the A549 and SK-MES-1 cell lines were determined using western blot (Fig. 2A) and semi-quantitative RT-PCR (Fig. 2B) analyses. Semi-quantitative RT-PCR analysis revealed that CD93 mRNA expression was high in A549 cells and low in the SK-MES-1 cells. The ratio of CD93 to GAPDH was obtained by normalizing the band intensities of CD93 to those of GAPDH at the protein level. The protein band for A549 cells showed a high signal, indicative of a high CD93 expression level (n=3), whereas the band for the SK-MES-1 cells showed a low signal, representing a low CD93 expression level.

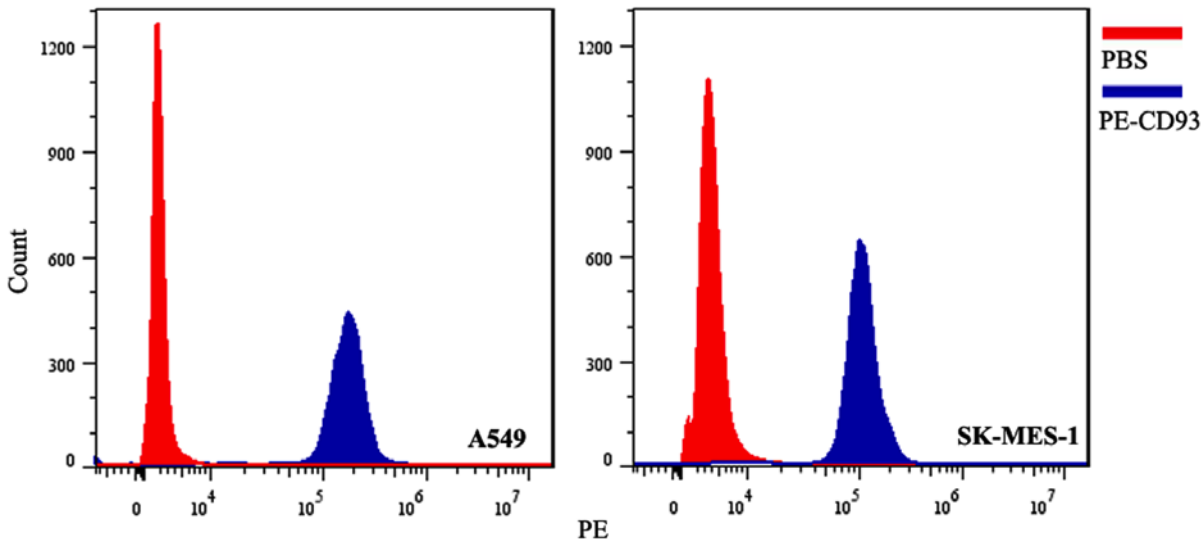

Figure 1. Flow cytometric analysis of A549 and SK-MES-1 cell lines. Each cell line was incubated with PBS (control; red) or phycoerythrin-CD93 (blue) to determine its level of CD93 expression.

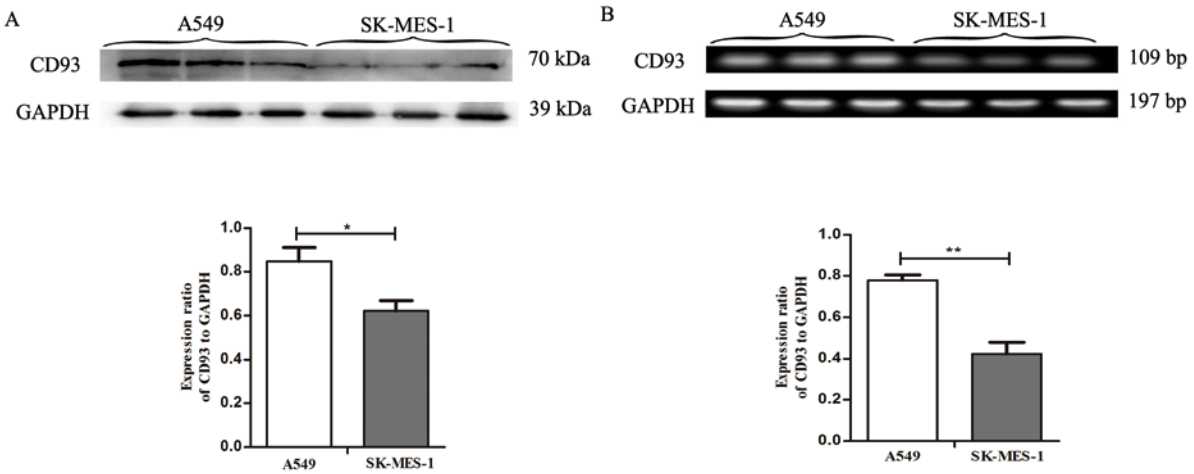

Figure 2. Quantification of CD93 mRNA and protein expression in non-small cell lung cancer cell lines. GAPDH was used as the internal reference. (A) Western blot verification of the differential expression of CD93 between A549 and SK-MES-1 cells. (B) Semi-quantitative reverse transcription-PCR analysis showed that CD93 mRNA expression was high in A549 cells and low the SK-MES-1 cells. *P<0.05, **P<0.01.

Radiochemical characteristics of the ^{125}I-anti-CD93 mAb. Labeling of the anti-CD93 mAb with ^{125}I resulted in a labeling yield of 91.37±2.21%, whereas labeling of the IgG yielded 90.24±1.58% ^{125}I-IgG. The radiochemical purity of both ^{125}I-anti-CD93 mAb and ^{125}I-IgG was >90%. The specific radioactivity of ^{125}I-anti-CD93 mAb was 1,096.44 MBq/mg, whereas that of ^{125}I-IgG was 1,082.88 MBq/mg. Both radiolabeled probes were relatively stable in human serum and in normal saline, where the radiochemical purity of these two probes was >90% for ≤72 h, with no significant difference between them (Fig. 3).

Cell-binding affinity of the ^{125}I-anti-CD93 mAb. The cell-binding studies indicated that the Kd of ^{125}I-anti-CD93 mAb was ~27.09±1.81 nM for A549 cells and 40.31±3.55 nM for SK-MES-1 cells (Fig. 4A), demonstrating that ^{125}I-anti-CD93 mAb had a higher binding affinity for A549 cells than for SK-MES-1 cells. In the competitive binding analysis (Fig. 4B), the excess unlabeled anti-CD93 mAb could almost completely block the binding of ^{125}I-anti-CD93 mAb, which was comparable with the 3-8% non-specific binding observed for ^{125}I-IgG.

Dynamic whole-body phosphor autoradiography. Whole-body phosphor autoradiography was performed at 24, 48 and 72 h after injection of the ^{125}I-anti-CD93 mAb into the A549 and SK-MES-1 tumor-bearing mice. The uptake of ^{125}I-anti-CD93 mAb in A549 tumor bearing mice increased from 24 h and declined at 72 h (Fig. 5; Table SI), with the highest uptake occurring at 48 h post-injection. At all times after injection, A549 tumors displayed a higher uptake of radioactivity compared with that of SK-MES-1 tumors. The radioactivity in the tumor area showed a substantial increase from 63,210±5,419 to 76,740±3,430 DLU/mm^2 for the A549

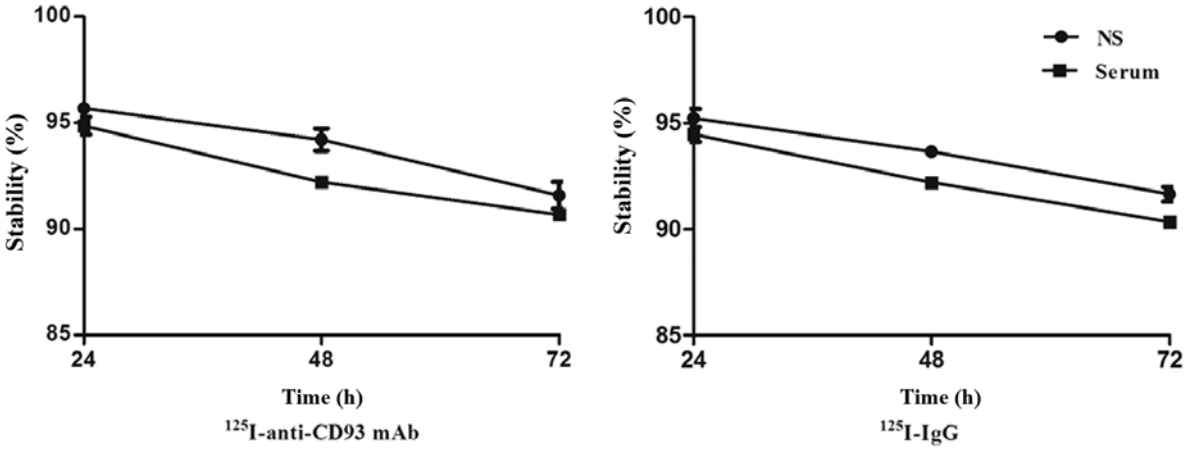

Figure 3. Stability analysis of the radiolabeled probes. Stability analysis of ^{125}I-anti-CD93 mAb and ^{125}I-IgG in human serum or NS at 24, 48 and 72 h. NS, normal saline; mAb, monoclonal antibody.

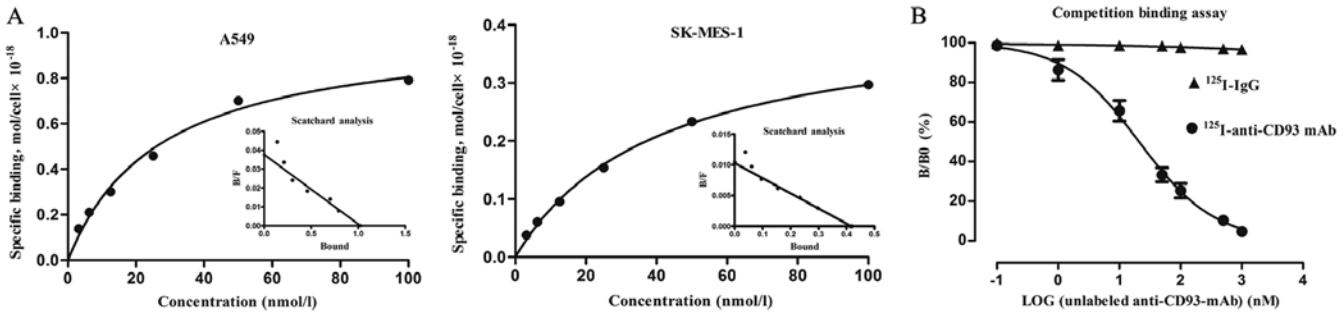

Figure 4. *In vitro* evaluation of the radiolabeled probes. (A) Representative saturation binding and Scatchard plots of ^{125}I-anti-CD93 mAb binding to non-small cell lung cancer cells. (B) The concentration of the labeled radioligand (anti-CD93 mAb and IgG isotope) was constant, while increasing concentrations of unlabeled anti-CD93 mAb were added to compete with the binding. mAb, monoclonal antibody. B/F, specific binding/free radioligand concentration; B/B0, radioactivity with the antibody-to-radioactivity without the antibody ratio.

model, whereas there was only an increase from 56,410±1991 to 57,060±3,495 DLU/mm^2 for the SK-MES-1 model. There was no obvious radioactivity concentration in ^{125}I-IgG group (i.e. A549-IgG group). ^{125}I-IgG could not delineate the tumor sites at any time point (Fig. 5), suggesting that there was a specific accumulation of ^{125}I-anti-CD93 mAb in the CD93-positive tumors only.

Biodistribution studies. Ex vivo biodistribution studies were performed to verify the results of the imaging studies and to further quantify the ^{125}I-anti-CD93 mAb uptake. As presented in Table I, ^{125}I-anti-CD93 mAb exhibited favorable blood clearance efficiency in A549 tumor xenograft models, comparable with the non-tumor-bearing mice (Table II). The uptake of ^{125}I-anti-CD93 mAb by A549 tumors was 7.81±0.80, 6.42±0.71 and 3.51±0.44% ID/g, with T/NT ratios of 2.42±0.14, 4.45±0.86 and 2.69±0.13 at 24, 48 and 72 h post injection, respectively. By contrast, the T/NT ratios of ^{125}I-anti-CD93 mAb in SK-MES-1 tumors were 1.67±0.27, 1.97±0.07 and 2.02±0.18 at 24, 48 and 72 h post injection, respectively, which were significantly lower than those in A549 tumors (Fig. 6 and Table III). The uptake of ^{125}I-IgG was only 1.71±0.24% ID/g at 48 h (Table IV), and the radioactive tracer failed to target CD93 in the tumor-bearing mice, suggesting the non-specific tumor binding of ^{125}I-IgG. Statistical comparisons of T/NT results (Table SII) further demonstrated the specificity of ^{125}I-anti-CD93 mAb *in vivo*. Bone, thyroid and intestines displayed minimal or background levels of ^{125}I-anti-CD93 mAb activity, in agreement with the imaging data.

Discussion

The identification of novel targeted molecules for specific tumors would increase the accuracy of cancer diagnosis. In recent years, radioimmunoimaging has emerged as a successful imaging tool for detecting different types of cancer (26,27). However, due to the lack of target molecules that can be uptaken in high quantities by tumor cells, the clinical application of radioimmunoimaging has been limited (28). Angiogenesis supplies all cellular tissues with oxygen and nutrients, and plays a key role not only during embryo development and physiological processes but also in several diseases, such as diabetes, ischemic heart disease, glomerular disease and cancer (29,30). Tumor angiogenesis occurs through the regulation of genes, including inhibitors of DNA binding-1, endothelial tyrosine kinase and CD34, that orchestrate endothelial sprouting and vessel maturation, including the deposition of a vessel-associated extracellular matrix (31). Angiogenic factors include

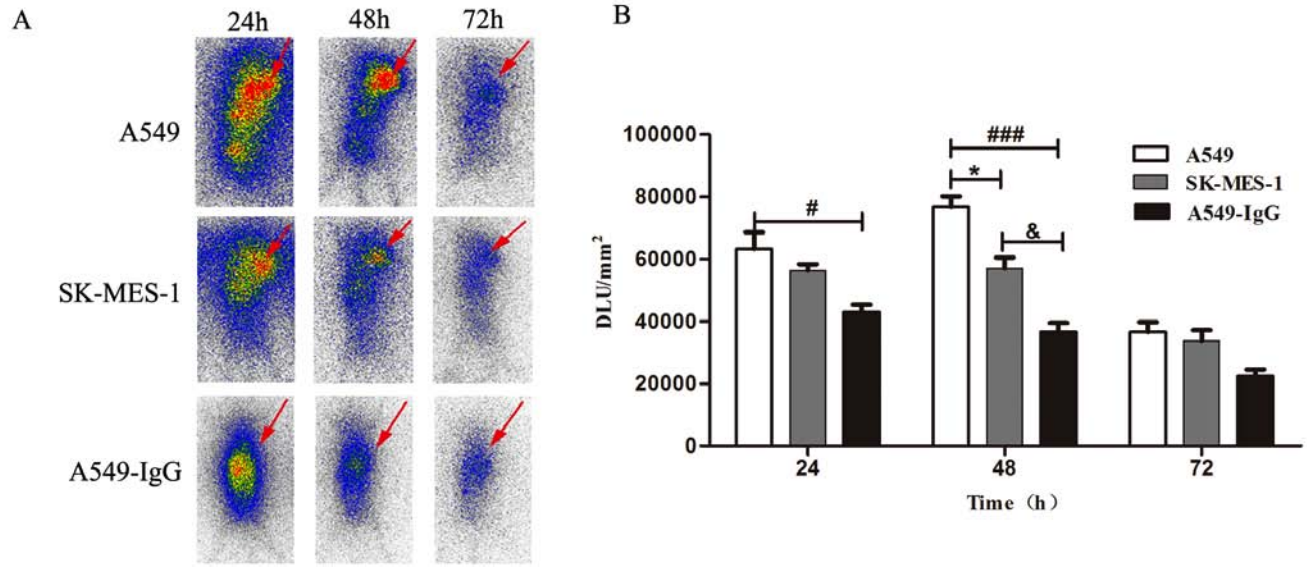

Figure 5. Whole-body phosphor autoradiographic images of non-small cell lung cancer tumor-bearing mice. (A) The uptake of ^{125}I-anti-CD93 mAb in the tumor area increased from 24 h and declined at 72 h, with the most notable accumulation in the tumor area at 48 h post-injection.^{125}I-IgG could not delineate the tumor sites at any time point. (B) Following injection of the ^{125}I-anti-CD93 mAb, the A549 tumors exhibited higher radiotracer uptake compared with that of SK-MES-1 tumors at all time points. The arrow points to the location of the tumor. *P<0.05; $^{\#}$P<0.05; $^{\&}$P<0.05;$^{\#\#\#}$P<0.001. . mAb, monoclonal antibody; DLU, digital light units.

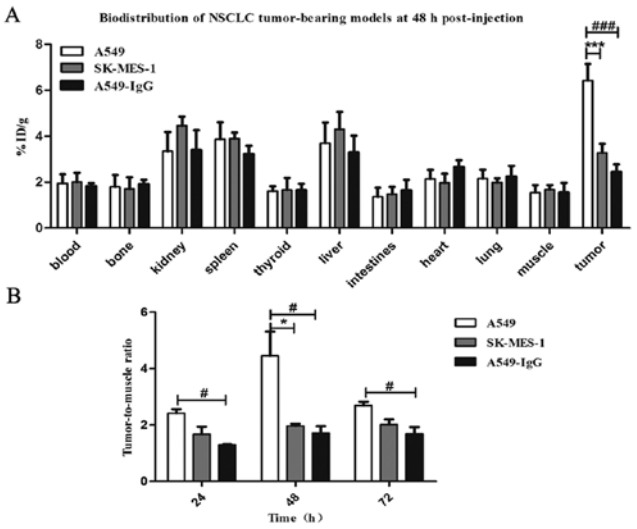

Figure 6. Biodistribution of ^{125}I-anti-CD93 mAb in non-small cell lung cancer tumor-bearing mice from 24 to 72 h post injection. (A) A549 tumors showed significantly higher uptake of ^{125}I-anti-CD93 mAb compared with that of SK-MES-1 tumors and the non-specific IgG group at 48 h. ***P<0.001 and $^{\#\#\#}$P<0.001. (B) The tumor-to-muscle ratio in the A549 group was higher compared with that in the SK-MES-1 and IgG control groups at 48 h. The highest tumor-to-muscle ratio in the A549 group occurred at 48 h post injection, in accordance with the results from whole-body phosphor autoradiography. *P<0.05; $^{\#}$P<0.05. . mAb, monoclonal antibody; % ID/g, percentage of injected dose per gram.

activator and inhibitor molecules that influence the angiogenic process (32).

CD93 has been recently reported as a novel angiogenic activator (21,33). Known as the complement component C1q receptor, CD93 is a transmembrane protein that is preferentially expressed in the vascular endothelium (34). Langenkamp *et al* (22) reported that high expression of CD93 promoted angiogenesis and reduced survival of patients with high-grade astrocytic gliomas. Moreover, it was reported that CD93 is highly expressed in nasopharyngeal carcinoma tissues and may serve as a novel therapeutic target for the treatment of this disease (35). Therefore, we postulated that CD93 may be a suitable biomarker for NSCLC.

Despite the evaluation of CD93 in relation to tumors would be of notable interest clinically, few studies on this topic have been conducted to date. Recent research shows that anti-CD93 mAb is able to neutralize the formation of new vessels both *in vitro* and *in vivo* (36), suggesting that it may be a suitable target for antiangiogenic therapy. The high blood clearance rate of anti-CD93 mAb demonstrated a low background in the plasma (36). Therefore, radiolabeled anti-CD93 mAb may provide an effective non-invasive method for visualizing CD93 expression *in vivo*. Similarly, in the present study, using a mouse model of lung cancer, the blood uptake of the administered ^{125}I-anti-CD93 mAb was lower compared with that of ^{125}I-IgG (Tables I and IV). Thus, ^{125}I-anti-CD93 mAb could be used in these NSCLC models, which is more clinically relevant compared with conventional tumor imaging agents.

In the *ex vivo* biodistribution experiment in the present study, low and uniform lung and cardiac uptakes also allowed for a higher contrast of the qualitative read on tumors. However, an unexpectedly high uptake (6.06±0.83% ID/g) in the spleen was observed 24 h after ^{125}I-anti-CD93 mAb administration. This may be due to the spleen being blood-rich and the biggest immune organ, which contained more CD93-positive immunocytes, so ^{125}I-anti-CD93 mAb in the blood may have more chances of binding to these immunocytes, leading to the relatively higher radioactivity retention. Considering that these CD93-positive immunocytes dispersed in white pulp of the spleen, the radioactive concentration was only slightly higher in the spleen. This diffused radioactivity had little effect on the lung cancer imaging. In addition, the radioactivity retention in the spleen was found to be time dependent. The uptake in the

Table I. Biodistribution of ^{125}I-antiCD93 monoclonal antibody in mice injected with A549 tumor cells.

	Time, h		
Tissue/organ, % ID/g[a,b]	24	48	72
Blood	3.37±0.74	1.95±0.38	0.96±0.99
Bone	2.20±0.55	1.79±0.52	0.76±0.36
Kidney	6.77±1.05	3.35±0.84	1.77±0.67
Spleen	6.06±0.83	3.87±0.74	2.58±0.32
Thyroid	2.30±0.48	1.61±0.20	1.17±0.21
Liver	4.82±1.07	3.70±0.90	1.44±0.58
Intestines	2.78±0.60	1.37±0.39	0.90±0.32
Heart	3.27±0.50	2.15±0.39	1.17±0.20
Lung	3.27±0.23	2.16±0.39	1.23±0.08
Muscle	3.30±0.55	1.54±0.34	1.31±0.16
Tumor	7.81±0.80[c]	6.42±0.71[c]	3.51±0.44[c]
Tumor-to-muscle ratio	2.42±0.14	4.45±0.86	2.69±0.13

[a]Mean ± SD. [b]% ID/g, the uptake of radioactivity in the tissues. [c]P<0.05.

Table II. Biodistribution of ^{125}I-antiCD93 monoclonal antibody in non-tumor-bearing mice.

	Time, h		
Tissue/organ, % ID/g[a,b]	24	48	72
Blood	3.57±0.22	1.89±0.20	0.97±0.87
Bone	2.35±0.41	1.74±0.48	0.81±0.29
Kidney	6.80±1.11	3.29±0.74	1.80±0.58
Spleen	6.02±0.47	3.95±0.63	2.49±0.32
Thyroid	2.22±0.35	1.70±0.11	1.10±0.20
Liver	4.77±1.01	3.81±0.84	1.39±0.55
Intestines	2.81±0.73	1.33±0.30	0.90±0.21
Heart	3.25±0.61	2.20±0.33	1.09±0.33
Lung	3.20±0.40	2.25±0.41	1.18±0.21
Muscle	3.24±0.47	1.50±0.40	1.25±0.18

[a]Mean ± SD. % ID/g, percentage of injected dose per gram. [b]% ID/g shows the uptake of radioactivity in the tissues.

spleen decreased to 3.87±0.74% ID/g at 48 h post injection, while 6.42±0.71% ID/g retention was found in the tumors at the same time point. Furthermore, there was no obvious radioactive accumulation in the spleen during whole-body phosphor autoradiography at 48 and 72 h post injection. ^{125}I-IgG was also evaluated in the present study, and it failed to target CD93 in the tumor-bearing mice, exhibiting non-specific retention in the tumors. These cell-specific and favorable non-target clearance features of ^{125}I-anti-CD93 mAb make it a promising radiotracer for imaging NSCLC.

Two NSCLC cell lines of different histological subtypes were selected for the present study: The human LUAD A549 cell line and the human LUSC SK-MES-1 cell line. Both LUSC and LUAD are the NSCLC subtypes occurring with the highest prevalence, accounting for 80-85% of all lung cancer cases (37,38). A large-scale sequencing study has revealed the genomic differences between LUAD and LUSC (39). These two subtypes show a number of different pathological characteristics, with LUAD growing more slowly than LUSC and tending to metastasize extensively at an earlier stage (40). A previous study has shown that patients with LUSC have a poorer prognosis compared with that of patients with LUAD following surgical resection (41). In addition, 4,124 genes were differentially expressed in LUAD and LUSC; a higher number of pathways associated with immune response, cell signal transduction, metabolism, cell division and cell proliferation were identified in LUAD compared with LUSC (42). Herein, the difference in CD93 expression between LUAD and LUSC has been described, with the levels being higher in A549 cells compared with those in SK-MES-1 cells. The

Table III. Biodistribution of ^{125}I-antiCD93 monoclonal antibody in mice with SK-MES-1 tumor cells.

	Time, h		
Tissue/organ, % ID/g[a,b]	24	48	72
Blood	3.40±0.67	2.01±0.40	1.04±0.06
Bone	2.27±0.42	1.70±0.51	0.70±0.21
Kidney	7.12±0.86	4.45±0.40	1.81±0.67
Spleen	6.25±0.59	3.89±0.27	2.74±0.45
Thyroid	2.62±0.19	1.66±0.53	1.18±0.13
Liver	5.03±1.17	4.31±0.75	1.50±0.41
Intestines	2.68±0.56	1.46±0.31	1.13±0.40
Heart	3.42±0.82	1.97±0.39	1.09±0.06
Lung	3.14±0.19	1.98±0.18	1.46±0.15
Muscle	3.06±0.47	1.67±0.21	1.31±0.14
Tumor	4.92±0.44[c]	3.27±0.40[c]	2.62±0.26[c]
Tumor-to-muscle ratio	1.67±0.27	1.97±0.07	2.02±0.18

[a]Mean ± SD. [b]% ID/g, the uptake of radioactivity in the tissues. [c]P<0.05.

Table IV. Biodistribution of ^{125}I-IgG isotype antibody in mice with A549 tumor cells.

	Time, h		
Tissue/organ, % ID/g[a,b]	24	48	72
Blood	3.45±0.70	1.82±0.14	1.09±0.11
Bone	2.71±0.30	1.91±0.19	1.13±0.15
Kidney	6.80±1.05	3.40±0.86	1.44±0.45
Spleen	4.42±0.87	3.23±0.35	1.68±0.37
Thyroid	2.70±0.43	1.65±0.28	0.85±0.13
Liver	6.05±0.84	3.29±0.73	1.40±0.29
Intestines	2.22±0.45	1.64±0.47	0.90±0.19
Heart	3.83±0.74	2.65±0.31	1.75±0.29
Lung	4.10±0.67	2.23±0.48	1.45±0.72
Muscle	3.13±0.23	1.54±0.43	0.90±0.06
Tumor	4.06±0.32	2.45±0.33	1.52±0.27
Tumor-to-muscle ratio	1.30±0.02	1.71±0.24	1.68±0.25

[a]Mean ± SD. [b]% ID/g, the uptake of radioactivity in the tissues.

specificity of a targeted probe based on CD93 expression in the two different NSCLC xenograft models was evaluated, and ^{125}I-anti-CD93 mAb revealed a higher rate of radiotracer retention in A549 tumors compared with that in SK-MES-1 tumors at all time points. The imaging parameters and their temporal changes may be essential for tissue characterization, including histological subtypes of cancers. Previous studies have demonstrated marked differences in positron emission tomography-CT parameters according to the histological subtype of resected NSCLC (43,44). In addition, various CT perfusion parameters have been reported to differ between lung cancer subtypes (45,46), showing inconsistent results (47-52). The results of the present study may be associated with the higher angiogenic potential of LUAD, as demonstrated by the higher level of CD93 expression in A549 cells compared with that in SK-MES-1 cells. These data indicated that CD93 may have the potential to be used as a biomarker for improving the accurate diagnosis of borderline lesions that lack specific characterizing features to distinguish their histological subtype.

Radioimmunoimaging reveals the accumulation of the target antibody *in vivo*, where the pharmacokinetic characteristics of the radiotracers are based on the molecular weight of the antibody (53). In the present study, full antibodies with a long circulating half-life were used. Fab fragments or genetically engineered antibodies may be an optimal choice for improving the poor pharmacokinetic characteristics of the

radiotracers (54,55). In addition, the molecular mechanism behind the regulation of CD93 expression in lung cancers of different histological subtype remains to be further investigated.

In conclusion, ^{125}I-anti-CD93 mAb could be used for non-invasive radioimmunoimaging of NSCLC based on tumor cell CD93 expression, particularly for histological subtype identification. Our results indicate the potential clinical application of this particular radiotracer for the diagnosis of CD93-positive tumors.

Acknowledgements

Not applicable.

Funding

The present study was supported by grants from the National Natural Science Foundation of China (grant no. 81000631), the National Natural Science Foundation of China (grant no. 81371601) and the Natural Science Foundation of Shandong Province (grant no. ZR2011HQ045).

Availability of data and materials

The datasets used and analyzed during the current study are available from the corresponding author on reasonable request.

Authors' contributions

WL wrote the manuscript. WL, CZ and DS performed the experiments. TL and GH designed the study and drafted the manuscript. WL, SZ and HC analyzed the data.

Ethics approval and consent to participate

All animal studies were conducted in accordance with protocols approved by the Animal Care and Use Committee of Shandong University.

Patient consent for publication

Not applicable.

Competing interests

The authors declare that they have no competing interests.

References

1. Molina-Pinelo S, Gutierrez G, Pastor MD, Her-Gueta M, Moreno-Bueno G, Garcia-Carbonero R, Nogal A, Suarez R, Salinas A, Pozo-Rodriguez F, *et al*: MicroRNA-dependent regulation of transcription in non-small cell lung cancer. PLoS One 9: e90524, 2014.
2. Schwander B, Ravera S, Giuliani G, Nuijten M and Walzer S: Cost comparison of second-line treatment options for late stage non-small-cell lung cancer: Cost analysis for Italy. Clinicoecon Outcomes Res 4: 237-243, 2012.
3. Boch C, Kollmeier J, Roth A, Stephan-Falkenau S, Misch D, Gruning W, Bauer TT and Mairinger T: The frequency of EGFR and KRAS mutations in non-small cell lung cancer (NSCLC): Routine screening data for central Europe from a cohort study. BMJ Open 3: e002560, 2013.
4. Raji OY, Duffy SW, Agbaje OF, Baker SG, Christiani DC, Cassidy A and Field JK: Predictive accuracy of the Liverpool Lung Project risk model for stratifying patients for computed tomography screening for lung cancer: A case-control and cohort validation study. Ann Intern Med 157: 242-250, 2012.
5. Didkowska J, Wojciechowska U, Mańczuk M and Łobaszewski J: Lung cancer epidemiology: Contemporary and future challenges worldwide. Ann Transl Med 4: 150, 2016.
6. Sharp A, Bhosle J, Abdelraouf F, Popat S, O'Brien M and Yap TA: Development of molecularly targeted agents and immunotherapies in small cell lung cancer. Eur J Cancer 60: 26-39, 2016.
7. Kumarakulasinghe NB, van Zanwijk N and Soo RA: Molecular targeted therapy in the treatment of advanced stage non-small cell lung cancer (NSCLC). Respirology 20: 370-378, 2015.
8. Spiegel ML, Goldman JW, Wolf BR, Nameth DJ, Grogan TR, Lisberg AE, Wong DJL, Ledezma BA, Mendenhall MA, Genshaft SJ, *et al*: Non-small cell lung cancer clinical trials requiring biopsies with biomarker-specific results for enrollment provide unique challenges. Cancer 123: 4800-4807, 2017.
9. Reck M: Pembrolizumab as first-line therapy for metastatic non-small-cell lung cancer. Immunotherapy 10: 93-105, 2018.
10. Majumder S and Chari ST: Chronic pancreatitis. Lancet 387: 1957-1966, 2016.
11. Knowles SM and Wu AM: Advances in immuno-positron emission tomography: Antibodies for molecular imaging in oncology. J Clin Oncol 30: 3884-3892, 2012.
12. Fu R, Carroll L, Yahioglu G, Aboagye EO and Miller PW: Antibody fragment and affibody immunoPET imaging agents: Radiolabelling strategies and applications. ChemMedChem 13: 2466-2478, 2018.
13. Li C, Wen B, Wang L, Feng H, Xia X, Ding Z, Gao B, Zhang Y and Lan X: ^{99}mTc-labeled single-domain antibody EG2 in targeting epidermal growth factor receptor. Nucl Med Commun 36: 452-460, 2015.
14. Mishani E, Abourbeh G, Eiblmaier M and Anderson CJ: Imaging of EGFR and EGFR tyrosine kinase overexpression in tumors by nuclear medicine modalities. Curr Pharm Des 14: 2983-2998, 2008.
15. Peña Y, Perera A and Batista JF: Immunoscintigraphy and radioimmunotherapy in Cuba: Experiences with labeled monoclonal antibodies for cancer diagnosis and treatment (1993-2013). MEDICC Rev 16: 55-60, 2014.
16. Weidner N: Intratumor microvessel density as a prognostic factor in cancer. Am J Pathol 147: 9-19, 1995.
17. Folkman J: The role of angiogenesis in tumor growth. Semin Cancer Biol 3: 65-71, 1992.
18. Folkman J: Angiogenesis. Annu Rev Med 57: 1-18, 2006.
19. Ribatti D: History of research on angiogenesis. Chem Immunol Allergy 99: 1-14, 2014.
20. Greenlee MC, Sullivan SA and Bohlson SS: Detection and characterization of soluble CD93 released during inflammation. Inflamm Res 58: 909-919, 2009.
21. Kao YC, Jiang SJ, Pan WA, Wang KC, Chen PK, Wei HJ, Chen WS, Chang BI, Shi GY and Wu HL: The epidermal growth factor-like domain of CD93 is a potent angiogenic factor. PLoS One 7: e51647, 2012.
22. Langenkamp E, Zhang L, Lugano R, Huang H, Elhassan TE, Georganaki M, Bazzar W, Loof J, Trendelenburg G, Essand M, *et al*: Elevated expression of the C-type lectin CD93 in the glioblastoma vasculature regulates cytoskeletal rearrangements that enhance vessel function and reduce host survival. Cancer Res 75: 4504-4516, 2015.
23. Lugano R, Vemuri K, Yu D, Bergqvist M, Smits A, Essand M, Johansson S, Dejana E and Dimberg A: CD93 promotes β1 integrin activation and fibronectin fibrillogenesis during tumor angiogenesis. J Clin Invest 128: 3280-3297, 2018.
24. Andersson H, Lindegren S, Bäck T, Jacobsson L, Leser G and Horvath G: Biokinetics of the monoclonal antibodies MOv 18, OV 185 and OV 197 labelled with 125I according to the m-MeATE method or the Iodogen method in nude mice with ovarian cancer xenografts. Acta Oncol 38: 323-328, 1999.
25. Sun H, Zhan Y, Liang T, Zhang C, Song J, Han J and Hou G: In vivo Toll-like receptor5 (TLR5) imaging with radiolabeled anti-TLR5 monoclonal antibody in rapamycin-treated mouse allogeneic skin transplantation model. Transpl Infect Dis 17: 80-88, 2015.
26. van Dongen GA, Visser GW, Lub-de Hooge MN, de Vries EG and Perk LR: Immuno-PET: A navigator in monoclonal antibody development and applications. Oncologist 12: 1379-1389, 2007.

27. Carmon KS and Azhdarinia A: Application of immuno-PET in antibody-drug conjugate development. Mol Imaging 17: 1536012118801223, 2018.
28. Ehlerding EB, England CG, Jiang D, Graves SA, Kang L, Lacognata S, Barnhart TE and Cai W: CD38 as a PET imaging target in lung cancer. Mol Pharm 14: 2400-2406, 2017.
29. Carmeliet P and Jain RK: Angiogenesis in cancer and other diseases. Nature 407: 249-257, 2000.
30. Carmeliet P: Angiogenesis in health and disease. Nat Med 9: 653-660, 2003.
31. Ribatti D: Judah Folkman, a pioneer in the study of angiogenesis. Angiogenesis 11: 3-10, 2008.
32. Otrock ZK, Mahfouz RA, Makarem JA and Shamseddine AI: Understanding the biology of angiogenesis: Review of the most important molecular mechanisms. Blood Cells Mol Dis 39: 212-220, 2007.
33. Khan KA, Naylor AJ, Khan A, Noy PJ, Mambretti M, Lodhia P, Athwal J, Korzystka A, Buckley CD, Willcox BE, *et al*: Multimerin-2 is a ligand for group 14 family C-type lectins CLEC14A, CD93 and CD248 spanning the endothelial pericyte interface. Oncogene 36: 6097-6108, 2017.
34. Greenlee MC, Sullivan SA and Bohlson SS: CD93 and related family members: Their role in innate immunity. Curr Drug Targets 9: 130-138, 2008.
35. Bao L, Tang M, Zhang Q, You B, Shan Y, Shi S, Li L, Hu S and You Y: Elevated expression of CD93 promotes angiogenesis and tumor growth in nasopharyngeal carcinoma. Biochem Biophys Res Commun 476: 467-474, 2016.
36. Orlandini M, Galvagni F, Bardelli M, Rocchigiani M, Lentucci C, Anselmi F, Zippo A, Bini L and Oliviero S: The characterization of a novel monoclonal antibody against CD93 unveils a new antiangiogenic target. Oncotarget 5: 2750-2760, 2014.
37. Cancer Genome Atlas Research Network: Comprehensive molecular profiling of lung adenocarcinoma. Nature 511: 543-550, 2014.
38. Cancer Genome Atlas Research Network: Comprehensive genomic characterization of squamous cell lung cancers. Nature 489: 519-525, 2012.
39. Campbell JD, Alexandrov A, Kim J, Wala J, Berger AH, Pedamallu CS, Shukla SA, Guo G, Brooks AN, Murray BA, *et al*: Distinct patterns of somatic genome alterations in lung adenocarcinomas and squamous cell carcinomas. Nat Genet 48: 607-616, 2016.
40. Hoda SA and Cheng E: Robbins basic pathology. Am J Clin Pathol, 2017.
41. Kawase A, Yoshida J, Ishii G, Nakao M, Aokage K, Hishida T, Nishimura M and Nagai K: Differences between squamous cell carcinoma and adenocarcinoma of the lung: Are adenocarcinoma and squamous cell carcinoma prognostically equal? Jpn J Clin Oncol 42: 189-195, 2012.
42. Liu J, Yang XY and Shi WJ: Identifying differentially expressed genes and pathways in two types of non-small cell lung cancer: Adenocarcinoma and squamous cell carcinoma. Genet Mol Res 13: 95-102, 2014.
43. Schuurbiers OC, Meijer TW, Kaanders JH, Looigen-Salamon MG, de Geus-Oei LF, van der Drift MA, van der Heijden EH, Oyen WJ, Visser EP, Span PN and Bussink J: Glucose metabolism in NSCLC is histology-specific and diverges the prognostic potential of ^{18}FDG-PET for adenocarcinoma and squamous cell carcinoma. J Thorac Oncol 9: 1485-1493, 2014.
44. Koh YW, Lee SJ and Park SY: Differential expression and prognostic significance of GLUT1 according to histologic type of non-small-cell lung cancer and its association with volume-dependent parameters. Lung Cancer 104: 31-37, 2017.
45. Graves EE, Maity A and Le QT: The tumor microenvironment in non-small-cell lung cancer. Semin Radiat Oncol 20: 156-163, 2010.
46. Shi J, Schmid-Bindert G, Fink C, Sadurski S, Apfaltrer P, Poilz LR, Liu B, Haberland U, Klotz E, Zhou C, *et al*: Dynamic volume perfusion CT in patients with lung cancer: Baselineperfusion characteristics of different histological subtypes. Eur J Radiol 82: e894-e900, 2013.
47. Ma SH, Xu K, Xiao ZW, Wu M, Sun ZY, Wang ZX, Hu ZG, Dai X, Han MJ and Li YG: Peripheral lung cancer: Relationship between multi-slice spiral CT perfusion imaging and tumor angiogenesis and cyclin D1 expression. Clin Imaging 31: 165-177, 2007.
48. Li Y, Yang ZG, Chen TW, Chen HJ, Sun JY and Lu YR: Peripheral lung carcinoma: Correlation of angiogenesis and first-pass perfusion parameters of 64-detector row CT. Lung Cancer 61: 44-53, 2008.
49. Sauter AW, Winterstein S, Spira D, Hetzel J, Schulze M, Mueller M, Pfannenberg C, Claussen CD, Klotz E, Hann von Weyhern C and Horger MS: Multifunctional profiling of non-small cell lung cancer using ^{18}F-FDG PET/CT and volume perfusion CT. J Nucl Med 53: 521-529, 2012.
50. van Elmpt W, Zegers CML, Reymen B, Even AJG, Dingemans AC, Oellers M, Wildberger JE, Mottaghy FM, Das M, Troost EGC and Lambin P: Multiparametric imaging of patient and tumor heterogeneity in non-small-cell lung cancer: Quantification of tumor hypoxia, metabolism and perfusion. Eur J Nucl Med Mol Imaging 43: 240-248, 2016.
51. Nakano S, Gibo J, Fukushima Y, Kaira K, Sunaga N, Taketomi-Takahashi A, Tsushima Y and Mori M: Perfusion evaluation of lung cancer: Assessment using dual-input perfusion computed tomography. J Thorac Imaging 28: 253-262, 2013.
52. Spira D, Neumeister H, Spira SM, Hetzel J, Spengler W, von Weyhern CH and Horger M: Assessment of tumor vascularity in lung cancer using volume perfusion CT (VPCT) with histopathologic comparison: A further step toward an individualized tumor characterization. J Comput Assist Tomogr 37: 15-21, 2013.
53. Kang F, Wang Z, Li G, Wang S, Liu D, Zhang M, Zhao M, Yang W and Wang J: Inter-heterogeneity and intra-heterogeneity of αvβ3 in non-small cell lung cancer and small cell lung cancer patients as revealed by ^{68}Ga-RGD2 PET imaging. Eur J Nucl Med Mol Imaging 44: 1520-1528, 2017.
54. Jing S, He Y, He Y, Wang L, Jia J, Shan X, Liu S, Tang M, Peng Z and Liu X: Imaging potential evaluation of fab derived from the anti-EGFRvIII monoclonal antibody 4G1. Radiat Res 190: 194-203, 2018.
55. Shi S, Orbay H, Yang Y, Graves SA, Nayak TR, Hong H, Hernandez R, Luo H, Goel S, Theuer CP, *et al*: PET imaging of abdominal aortic aneurysm with ^{64}Cu-labeled anti-CD105 antibody fab fragment. J Nucl Med 56: 927-932, 2015.